Structure, Volume *22*

Supplemental Information

The Mitochondrial Fission Receptor MiD51 Requires ADP as a Cofactor

Oliver C. Losón, Raymond Liu, Michael E. Rome, Shuxia Meng, Jens T. Kaiser, Shu-ou Shan, and David C. Chan

SUPPLEMENTAL FIGURES

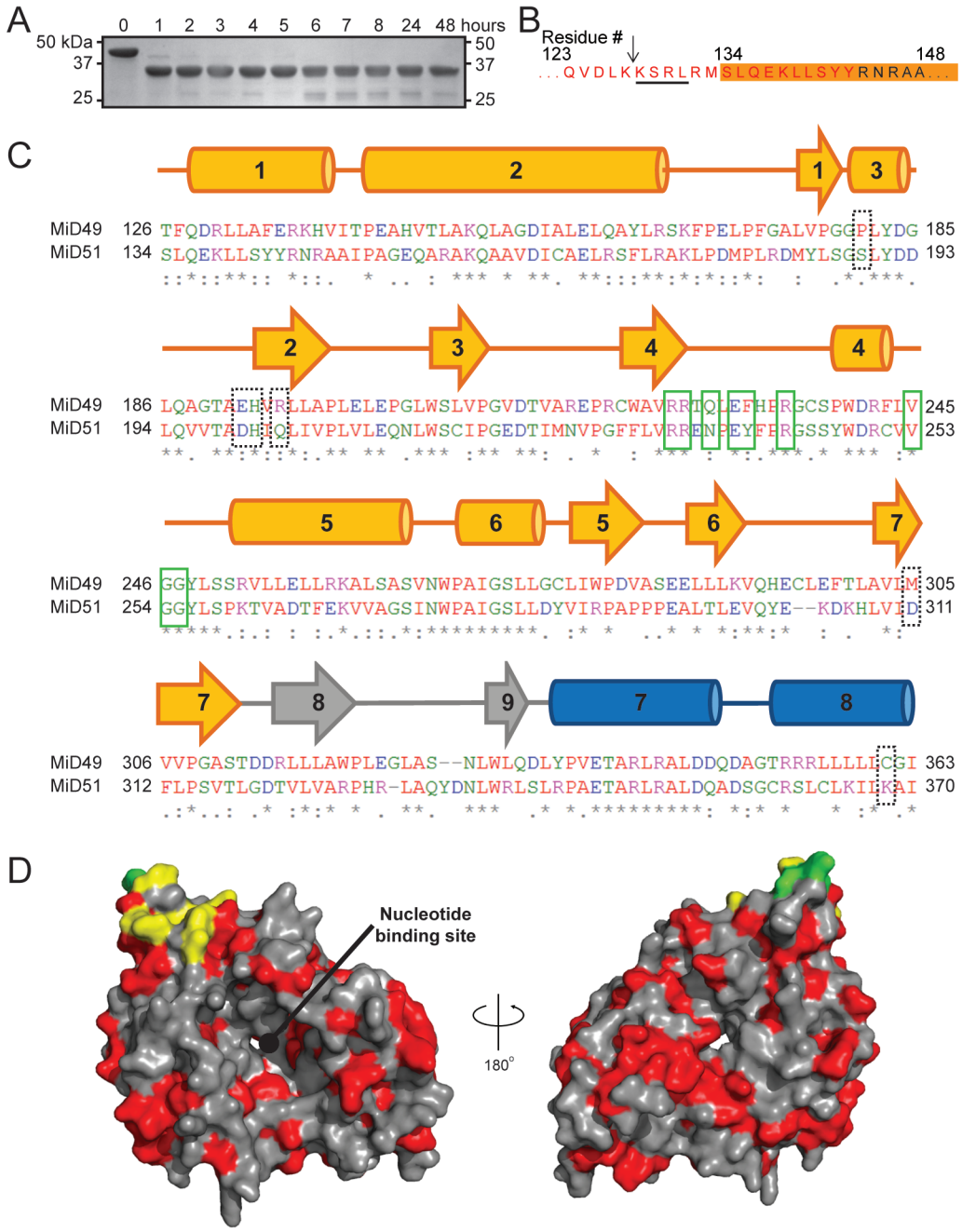

Figure S1, related to Figure 1. (A, B) Identification of a stable MiD51 domain. (A) Limited trypsin proteolysis of MiD51Δ1-48 produces a stable fragment that is resistant to proteolysis over two days. Proteolysis products were analyzed by SDS-PAGE. (B) Details of the stable domain. The sequence of MiD51 protein at the C-terminal end of the non-regular secondary structure (NRSS) segment is shown. NRSS sequence is depicted in red, and the black arrow indicates the trypsin site. N-terminal sequencing identified the underlined residues. The orange shading denotes the N-terminal sequence of the crystallized segment. (C) Protein sequence

alignment for *Mus musculus* MiD49 and MiD51. The dashed boxes highlight residues in MiD51 involved in nucleotide binding. The green boxes highlight conserved residues for Drp1 binding. Residue chemistries are depicted by their color. Red, small and/or hydrophobic; blue, acidic; magenta, basic; green, sulfhydryl, hydroxyl or amine containing and glycine. Sequence similarity symbols: asterisk, fully conserved; colon, highly conserved; period, weakly conserved. Protein secondary structure topology from the MiD51 model is depicted above the sequence. α-helix and strand numbering and coloring are done as in Fig. 1A. (D) Surface representation of mouse MiD51Δ1-133 with MiD49 conserved residues depicted in red. Yellow residues are MiD49 conserved residues that are important for Drp1 binding. Green residues are residues important for Drp1 binding that are not conserved.

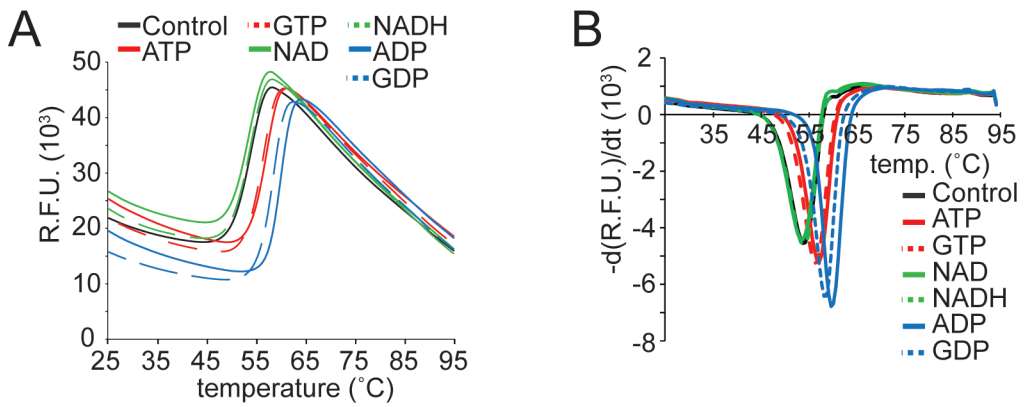

C

- Mg $^{2+}$ reactions

	Control	ATP	AMPPNP	ADP	AMP	cAMP	GTP	GDP	GMP	cGMP	CTP	CDP	UTP	TTP	TDP	UDP	NAD	NADH
1 mM	—	55.3±0.3	54.5±0.0	58.5±0.0	54.2±0.3	54.0±0.0	55.0±0.0	56.5±0.0	54.2±0.3	54.0±0.0	55.2±0.4	55.2±0.3	55.3±0.8	55.0±0.0	54.6±0.2	54.6±0.2	54.0±0.0	54.0±0.0
5 mM	—	56.9±0.2	55.5±0.0	59.8±0.3	54.5±0.0	54.0±0.0	56.0±0.0	58.3±0.3	54.3±0.3	54.2±0.3	55.3±1.3	55.2±0.8	54.8±0.8	56.0±0.0	55.1±1.0	55.1±0.7	54.0±0.0	54.0±0.0
10 mM	54.3	57.5±0.0	56.2±0.3	60.3±0.3	54.9±0.2	54.0±0.0	56.6±0.2	58.9±0.2	54.5±0.0	53.8±0.3	56.3±0.8	55.9±0.7	55.7±0.8	56.5±0.0	56.1±0.9	56.1±0.8	54.0±0.0	54.1±0.2

D

+ Mg $^{2+}$ reactions

	Control	ATP	AMPPNP	ADP	AMP	cAMP	GTP	GDP	GMP	cGMP	CTP	CDP	UTP	TTP	TDP	UDP	NAD	NADH
1 mM	—	54.5±0.0	54.0±0.0	57.1±0.2	54.1±0.2	53.9±0.2	54.3±0.3	55.7±0.3	54.0±0.0	54.0±0.0	54.2±0.4	54.1±0.5	53.4±0.3	54.2±0.3	54.3±0.3	54.3±0.3	54.0±0.0	54.1±0.2
5 mM	—	56.4±0.2	55.1±0.2	59.5±0.0	54.3±0.3	53.8±0.3	55.5±0.0	57.9±0.2	54.2±0.3	53.8±0.3	54.2±0.8	55.0±0.4	54.9±0.5	55.6±0.2	55.5±0.4	55.5±0.4	54.0±0.0	54.4±0.2
10 mM	54.0	57.1±0.2	56.0±0.0	60±0.0	54.5±0.0	53.8±0.3	56.4±0.2	58.5±0.0	54.5±0.0	53.8±0.3	54.2±1.1	55.5±0.5	55.8±0.5	56.3±0.3	56.0±0.5	56.0±0.7	54.1±0.2	54.0±0.0

E

+ Mg $^{2+}$ reactions

	Control	ATP	ADP	AMP	cAMP	GTP	GDP	GMP	cGMP	CTP	CDP	UTP	UDP	NAD	NADH
10 mM	45.9±0.2	46.0±0.0	45.5±0.0	44.8±0.3	45.8±0.3	45.8±0.3	45.3±0.3	46±0.0	45.5±0.0	45.5±0.0	45.9±0.2	45.5±0.0	45.0±0.0	45.0±0.3	45.2±0.3

Figure S2, related to Figure 2. Screening for potential MiD51 ligands. (A-D) In the thermal shift assay, thermal denaturation of MiD51 causes dequenching of Sypro Orange. As a result, increases in Sypro Orange fluorescence report protein unfolding. (A) Raw fluorescence traces from representative groups. (B) The protein melting temperature is determined by calculating the first derivative for each fluorescence trace. (C) MiD51Δ1-133 melting temperatures in the presence of the indicated nucleotides without Mg^{2+}. (D) MiD51Δ1-133 melting temperatures in the presence of the indicated nucleotides with Mg^{2+}. (E) MiD49Δ1-124 melting temperatures in the presence of the indicated nucleotides with Mg^{2+}. Melting temperatures in (C) through (E) are averages from three independent experiments ± standard deviation.

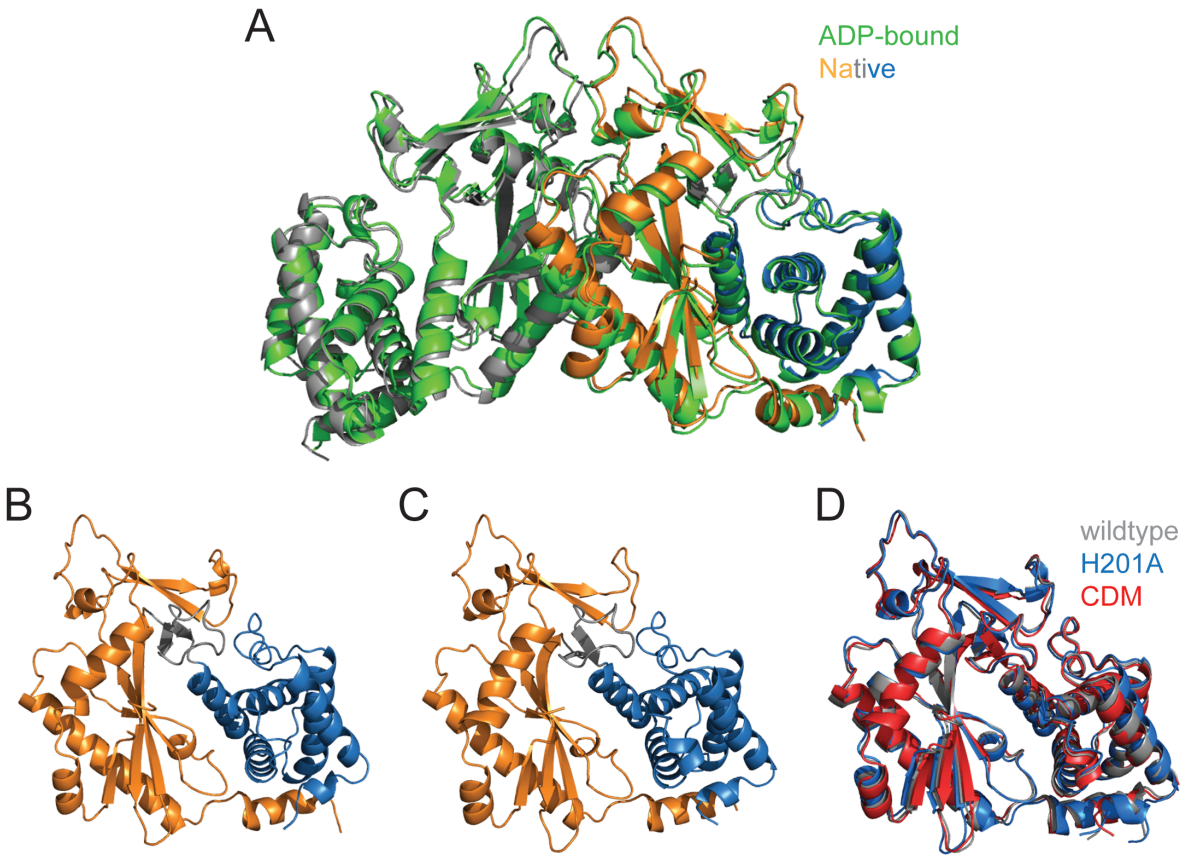

Figure S3, related to Figure 3. (A) Structural alignment of native MiD51Δ1-133 and ADP-bound dimers. The native (apo) dimer is colored as in Fig. 3, and the ADP-bound dimer is colored green. (B) Ribbon representation of MiD51Δ1-133 H201A (nucleotide-binding mutant). (C) Ribbon representation of compound dimer mutant of MiD51Δ1-133. Models in (B) and (C) are colored as in Fig. 1B. (D) Superimposition of MiD51Δ1-133 wildtype (gray), H201A (blue) and compound dimer mutant (CDM, red).

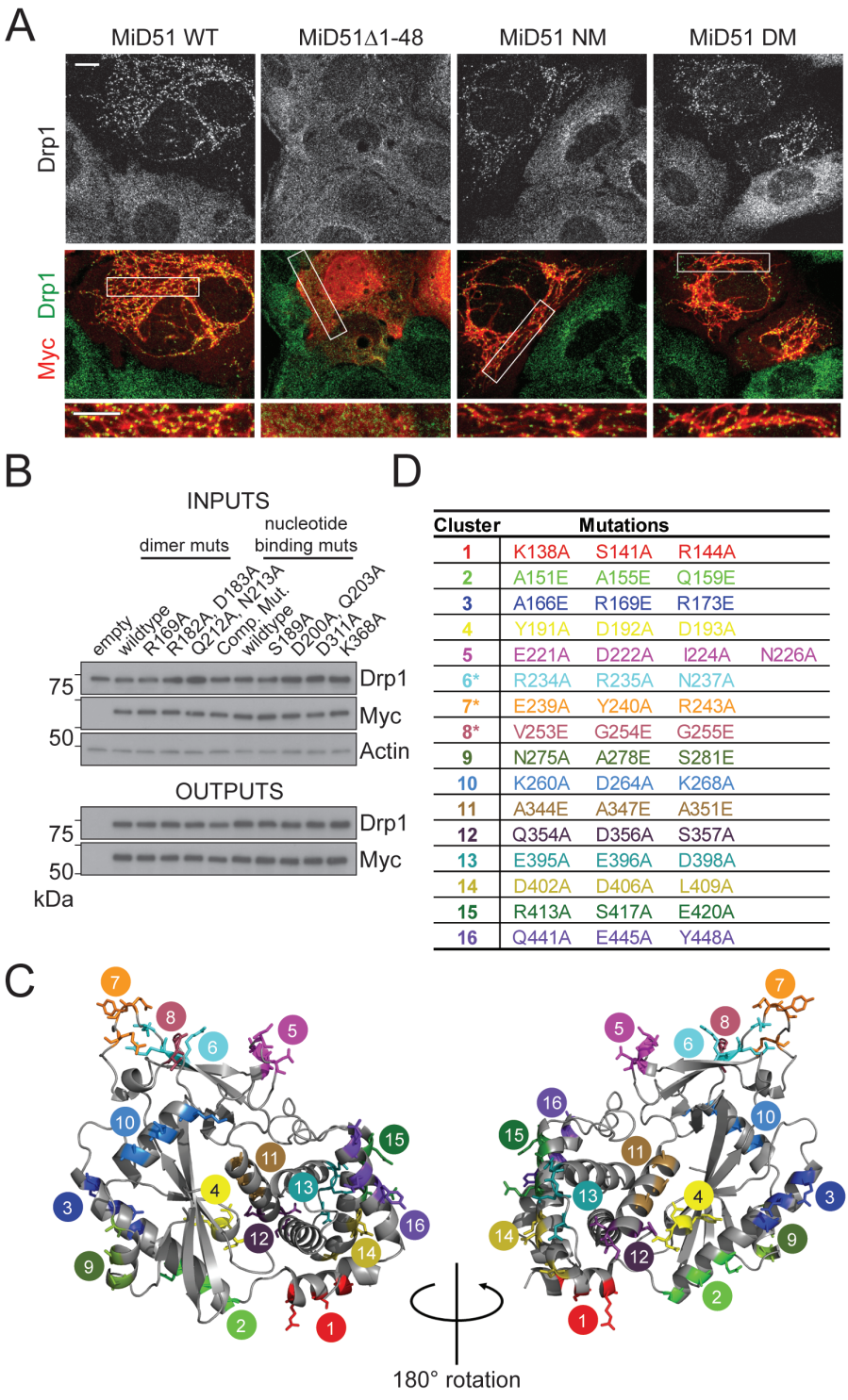

Figure S4, related to Figure 4. Identification of the Drp1 binding site on MiD51. (A) Effect of MiD51 nucleotide-binding and dimerization mutations on Drp1 recruitment to mitochondria. *Fis1/Mff*-null MEFs were transfected with the indicated MiD51-Myc construct, and Drp1 localization was visualized by immunostaining. Transfected cells were determined by an anti-Myc antibody. MiD51Δ1-48 lacks the transmembrane domain and does not localize to

mitochondria. Scale bars, 10 μm. White boxes delineate bottom inset boundaries. NM, nucleotide-binding site mutant (S189A); DM, compound dimer mutant. (B) Co-immunoprecipitation of MiD51 mutants with Drp1. Drp1 was co-transfected with either empty vector or Myc tagged MiD51 mutant constructs. Cells were treated with a reversible crosslinker and solubilized before immunoprecipitation. The output panels show Drp1 association with the anti-Myc immunoprecipitates. The top panels show expression of MiD51-Myc and Drp1 in the cell lysates. Actin is a loading control. (D) A tabulation of the 16 cluster mutants. Cluster mutants that perturb Drp1 binding are indicated with asterisks. (D) Structural depiction of the cluster mutants. The mutants were designed to systematically probe the solvent-exposed surface of MiD51. Three clusters showed significant loss of Drp1 binding (6, 7 and 8).

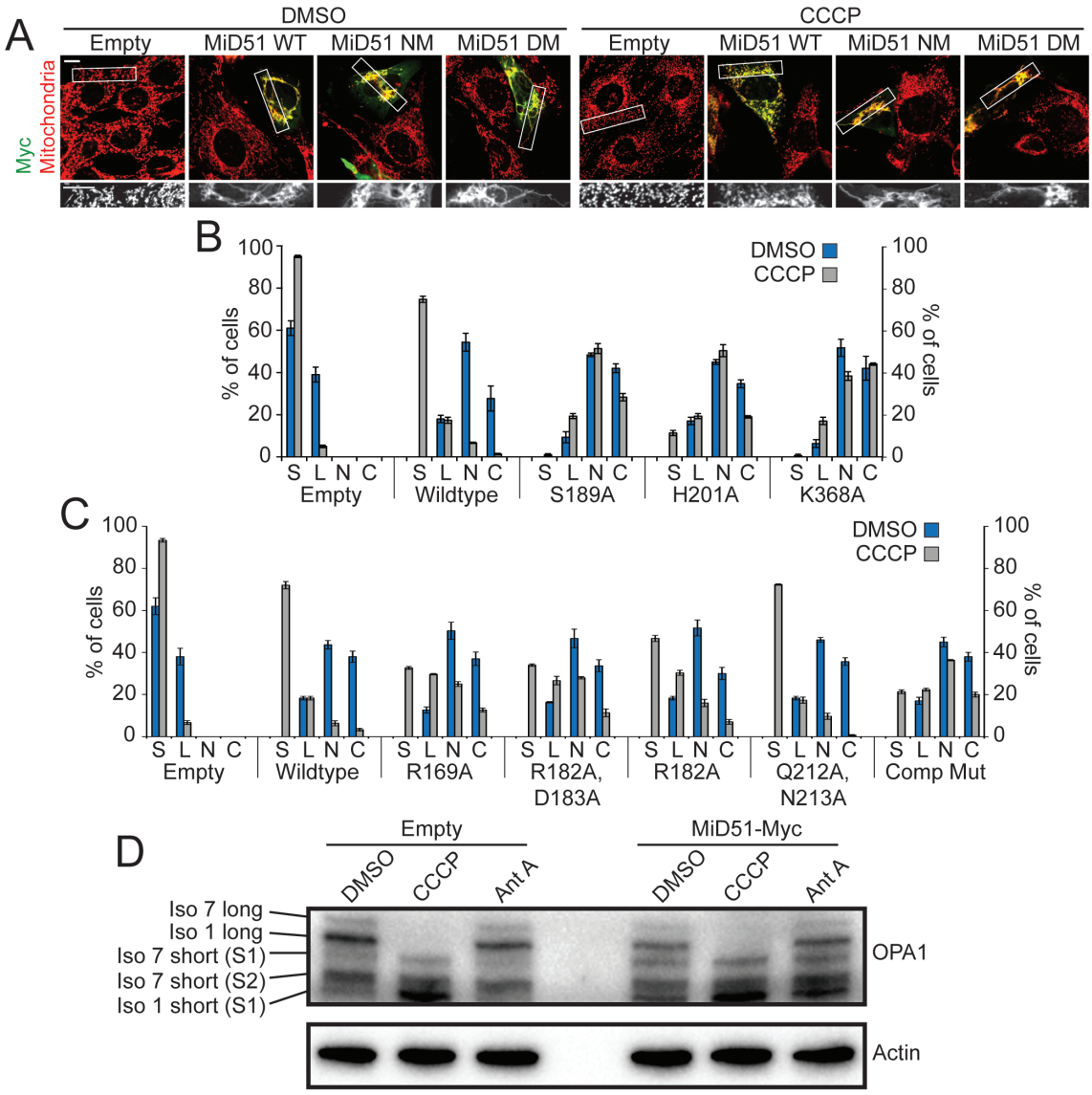

Figure S5, related to Figure 5. MiD51 nucleotide-binding site and dimerization mutants are defective in CCCP-induced mitochondrial fragmentation. (A) Fission activity of MiD51 variants. MEFs were transfected with empty vector or the indicated MiD51 construct and treated with vehicle or CCCP. Transfected cells were identified with an anti-Myc antibody, and mitochondria were highlighted with an anti-Tom20 antibody. (B) Quantification of mitochondrial morphology for nucleotide-binding site mutants. (C) Quantification of mitochondrial morphology for dimerization mutants. Comp Mut, compound mutant containing 5 substitutions at the dimer interface. Data in (B) and (C) are averages from three independent experiments ± standard deviation. Mitochondrial morphology scoring: S, short; L, long; N, net-like; C, collapsed. Scale bars, 10 µm. The regions within the white boxes are shown at higher magnification below. (D) Proteolytic processing of OPA1 analyzed by Western blotting of cell lysates Loss of membrane potential during CCCP treatment causes activation of Oma1 mediated cleavage at site 1 (S1) in both isoforms 1 and 7 (Ehses et al., 2009; Head et al., 2009). Cleavage at S2 is mediated by Yme1 and is insensitive to loss of membrane potential (Griparic et al., 2007; Song et al., 2007). CCCP treatment causes increased processing of OPA1, but antimycin A treatment does not. Actin is a loading control.

SUPPLEMENTAL REFERENCES

Ehses, S., Raschke, I., Mancuso, G., Bernacchia, A., Geimer, S., Tondera, D., Martinou, J.C., Westermann, B., Rugarli, E.I., and Langer, T. (2009). Regulation of OPA1 processing and mitochondrial fusion by m-AAA protease isoenzymes and OMA1. J Cell Biol *187*, 1023-1036.

Griparic, L., Kanazawa, T., and van der Bliek, A.M. (2007). Regulation of the mitochondrial dynamin-like protein Opa1 by proteolytic cleavage. J Cell Biol *178*, 757-764.

Head, B., Griparic, L., Amiri, M., Gandre-Babbe, S., and van der Bliek, A.M. (2009). Inducible proteolytic inactivation of OPA1 mediated by the OMA1 protease in mammalian cells. J Cell Biol *187*, 959-966.

Song, Z., Chen, H., Fiket, M., Alexander, C., and Chan, D.C. (2007). OPA1 processing controls mitochondrial fusion and is regulated by mRNA splicing, membrane potential, and Yme1L. J Cell Biol *178*, 749-755.